Guidance Scheme for a Mach 3 Staged Gliding Booster

J. Christopher Naftel* and Richard W. Powell*
NASA Langley Research Center, Hampton, Virginia 23665

One of the promising launch concepts that could replace the current Space Shuttle launch system is a two-stage, winged, vertical-takeoff, parallel-burn, fully reusable launch vehicle comprised of a manned orbiter and an unmanned booster. During the boost phase of ascent, the booster provides propellant for the orbiter engines through a cross-feed system. When the vehicle reaches Mach 3, the booster propellants are depleted and the booster is staged and glides to a horizontal landing at a launch site runway. One of the major design issues for this class of vehicle is the unpowered glide back of the booster after the staging maneuver is completed. A guidance algorithm was developed for the glide-back maneuver and verified using a three-degree-of-freedom trajectory simulation that included static trim in pitch. The guidance algorithm was tested using off-nominal atmospheric, staging, and booster aerodynamic characteristics.

Nomenclature

A_n = normal acceleration, g
b = reference span, ft
C_D = drag coefficient, = drag/$q_\infty S_{ref}$
C_L = lift coefficient, = lift/$q_\infty S_{ref}$
c = reference chord, ft
h = altitude, ft
$\dot{h}$ = d h/d t, ft/s
I_{sp} = specific impulse, s
L_{ref} = reference length, ft
M = Mach number
q_∞ = dynamic pressure, psf
S_{ref} = reference area, ft^2
V = atmospheric relative velocity, ft/s
W_{ew} = east-west wind component (wind toward the east positive), ft/s
X_{rt}, Y_{rt} = vehicle position relative to runway threshold, ft
$\dot{X}_{rt}, \dot{Y}_{rt}$ = vehicle velocity relative to runway threshold, ft/s
α = angle of attack, deg
γ = atmospheric relative flight-path angle, deg
δ_e = elevon deflection (positive trailing-edge down), deg
ρ = atmospheric density, slug/ft^3
ρ_{76} = 1976 standard atmospheric density, slug/ft^3
σ = standard deviation
ϕ = roll angle, deg

Introduction

RECENT studies of launch vehicles that are designed to replace the current Space Shuttle launch system have included a two-stage, winged, fully reusable, vertical-takeoff, parallel-burn, launch vehicle concept.[1-4] This concept incorporates an unmanned booster that stages from a manned orbiter at Mach 3, glides back unpowered to the launch site vicinity, and lands horizontally on a runway. Mach 3 was chosen for staging for two major reasons. The first reason is that Mach 3 is the highest Mach number that would allow an unpowered return to the launch site with adequate performance reserves.[5] This unpowered return eliminates the need for air-breathing propulsion on the booster, which is a complex subsystem that would require maintenance and checkout before every launch. The second reason is that if staging occurred at a higher Mach number the booster would experience an increased level of aerodynamic heating that would require a thermal protection system.

Two issues, the staging maneuver and booster glide back, are critical to the feasibility of this two-stage concept. A staging maneuver analysis has been completed and is presented in Ref. 6. For the booster glide-back analysis, which is presented in this paper, a guidance algorithm was developed and incorporated into a three-degree-of-freedom trajectory computer program. Glide-back simulations were performed with many off-nominal conditions including atmospheric density dispersions, errors in predicted aerodynamics, and errors in staging state conditions.

Launch Vehicle Description

Ascent Configuration Characteristics

The two-stage, fully reusable launch vehicle concept analyzed in this investigation is shown in Fig. 1. Table 1 shows the major characteristics of each stage. Both the booster and orbiter engines use liquid hydrogen and liquid oxygen as propellants. During the boost phase, the orbiter uses propellant that is cross fed from the booster. After staging, the orbiter uses

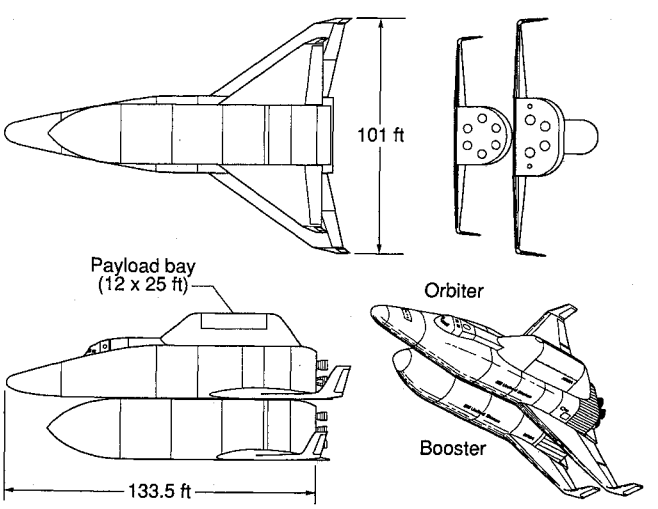

Fig. 1 Two-stage, fully reusable concept.

Presented as Paper 90-0223 at the AIAA 28th Aerospace Sciences Meeting, Reno, NV, Jan. 8-11, 1990; received Feb. 11, 1990; revision received Nov. 5, 1990; accepted for publication Nov. 13, 1990.

*Aerospace Engineer, Space Systems Division, Mail Stop 365. Member AIAA.

Table 1 Characteristics of orbiter and booster

	Orbiter	Booster
Gross weight, lb	1,186,872	960,636
Dry weight, lb	152,971	107,362
Number of engines	4	6
Engine thrust_{VAC}, lb	352,000	352,000
Engine I_{sp}, sec	438	438
Engine exit area, ft^2	34.3	34.3
S_{ref}, ft^2	3772.6	3291.2
L_{ref}, ft	133.5	119.7
c, ft	50.2	43.5
b, ft	101.2	84.8

propellant supplied from internal tanks. The launch pad is assumed to be a modified Space Shuttle launch pad at the Kennedy Space Center (KSC). The details of the nominal ascent trajectory are discussed in Ref. 6. The orbiter can deliver up to 20,000 lb of payload to a 220-n.mi. circular orbit, inclined 28.5 deg. The payload is carried on the back of the orbiter in an external canister arrangement. Both the booster and orbiter land horizontally at the KSC Shuttle Orbiter landing strip at the completion of their mission.

Booster Characteristics

The aerodynamic data base for a representative configuration of the booster stage is presented in Ref. 7. The booster's control surfaces include elevons and tip fin controllers. The elevons are used for both pitch and roll control. This is accomplished by differentially deflecting the elevons so that they can function as both elevators and ailerons. Thus, the elevons are used to control both angle of attack and roll angle. The elevons have deflection limits of +20 and −30 deg. The tip fin controllers are used to control sideslip angle and can function as speed brakes. The tip fin controllers have deflection limits of ±60 deg. The booster's wings are designed to accommodate up to a 2.5-g normal acceleration based on the booster return weight. The landing gear on the booster is designed for a sideslip angle limit of ±3 deg, and a maximum descent rate of 3 ft/s at touchdown.

Computational Tools

Program to Optimize Simulated Trajectories

The glide-back trajectories presented were generated with the three-degree-of-freedom version of the Program to Optimize Simulated Trajectories (POST).[8] POST is a generalized point mass, discrete parameter targeting and optimization program with the capability to target and optimize trajectories for a powered or unpowered vehicle near a rotating oblate planet. POST is an event-oriented trajectory program that can be used to analyze ascent, on-orbit, entry, and atmospheric trajectories. Any calculated variable in POST can be optimized while subjected to a combination of both equality and inequality constraints. After several modifications were made to POST, it was used in a simulation mode for the booster glide-back trajectories. These modifications include the addition of the closed-loop guidance algorithm that was developed for the booster's glide back to the launch site runway, the addition of the booster aerodynamic data base, and the addition of numerous atmospheres and wind profiles.

Table 2 Nominal conditions at staging maneuver completion

Altitude, ft	88,287
V, ft/s	2,732
γ, deg	30.0
α, deg	−10.0
Range, n.mi.	15.8
q, psf	204.0
Mach number	2.78

Global Reference Atmosphere Model

The Global Reference Atmosphere Model (GRAM)[9] was used to model the atmospheres and wind profiles that were used to evaluate the booster glide-back guidance algorithm. The GRAM is an engineering model atmosphere that includes mean values for density, temperature, pressure, and wind components, and density perturbation magnitudes and random perturbation profiles for density variations along a specified trajectory. The atmospheric data is a function of latitude, longitude, altitude, and date. The capability in GRAM that allows for the simulation of random perturbation profiles about mean conditions[10] was utilized in this study. This feature allows for the simulation of a large number of realistic density profiles along a reference trajectory through the atmosphere, with realistic values of peak perturbation values.

Booster Glide-Back Guidance Analysis

For the glide-back analysis, a guidance algorithm was developed, a nominal glide-back trajectory was defined, and the guidance technique was tested with various atmospheric dispersions and other off-nominal conditions.

Guidance Algorithm

The guidance algorithm developed for the booster's glide back is divided into six phases, beginning at the completion of the staging maneuver and ending at touchdown on the runway (Fig. 2). The overall strategy of the different phases includes arresting the booster's downrange motion by turning back toward the launch area, depleting the booster's excess energy, intersecting a heading alignment cylinder (HAC), flying on the HAC until lined up with the KSC Shuttle runway, performing a flare maneuver, and landing on the runway.

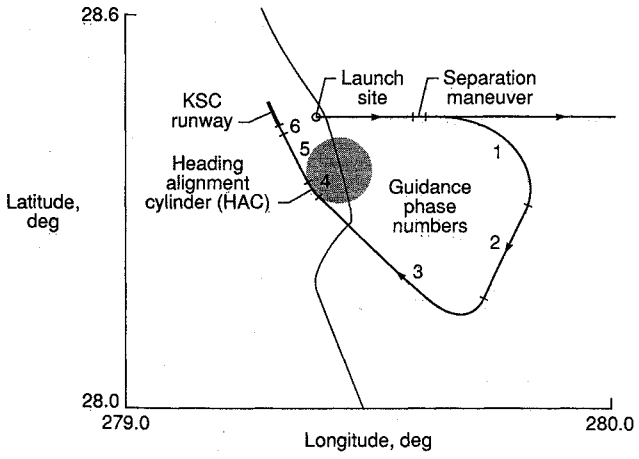

Fig. 2 Booster glide-back guidance phases.

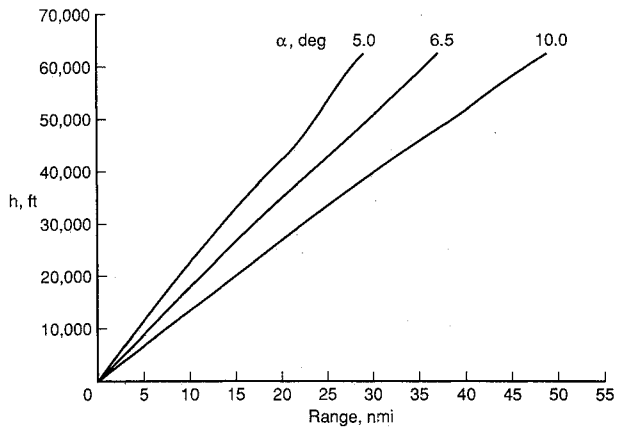

Fig. 3 Booster's potential range.

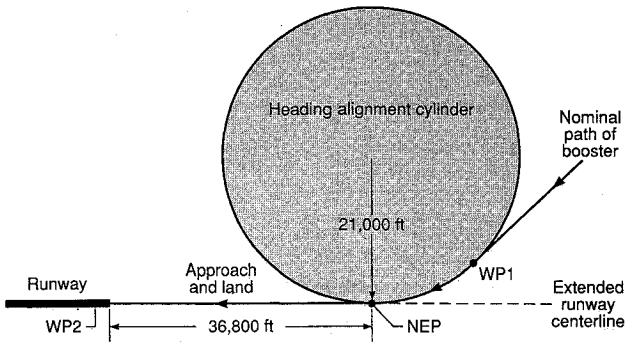

Fig. 4 Heading alignment cylinder geometry.

Phase 1—Initial Turn After Staging Maneuver

Table 2 gives the trajectory conditions for the booster at the completion of the nominal staging maneuver. The first phase, which begins at the completion of the staging maneuver, is the maneuver that arrests the downrange motion of the booster and turns it back toward the runway. Before the turn begins, the booster has a heading angle of 90 deg; when the turn is completed, the booster has a heading angle of 210 deg. The heading angle of the runway is 330 deg.

The POST program was used to find the optimal (minimum time) phase-1 turning maneuver with the appropriate initial and final heading angles and a maximum normal acceleration of 2.3 g. Since the booster has a maximum normal acceleration limit of 2.5 g, a margin of 0.2 g was established to handle the expected off-nominal conditions. An open-loop approximation to the optimal turning maneuver was modeled in which the angle of attack was a function of Mach number and the roll angle was a function of heading angle.

Phase 2—Excess Performance Dissipation

When the booster reaches a heading angle of 210 deg, phase 2 begins and the booster is rolled to 0 deg at a rate of 20 deg/s. The roll angle is then modulated by feedback to keep the booster on a 210-deg heading angle. The angle of attack continues to follow the Mach number schedule used in phase 1 until an angle of attack of 6.5 deg is reached. For the remaining portion of phase 2, the angle of attack is kept at 6.5 deg.

The purpose of phase 2 is to deplete the booster's excess performance. The guidance algorithm continuously calculates the range from the booster's current position to the target point on the runway. The guidance algorithm also calculates the booster's potential range at its current altitude and angle of attack using the plot found in Fig. 3. Once the booster's potential range to the runway is equal to the actual range to the runway, the third guidance phase is initiated.

Phase 3—Heading Alignment Cylinder Acquisition

Phase 3 consists of the turn and glide to the HAC. Throughout phase 3, the angle of attack is modulated by feedback about the nominal angle of attack of 6.5 deg to keep the booster's actual range to the runway equal to its potential range. The booster has approximately equal range margins above and below its potential range at an angle of attack of 6.5 deg. The upper performance limit is defined by the booster's maximum L/D, which occurs at an angle of attack of 10 deg. The lower performance limit was defined at an angle of attack of 5 deg. Figure 3 shows the booster's potential range for angles of attack between 5 and 10 deg.

During phase 3, the booster's roll angle is modulated to keep the booster headed toward way-point 1 (WP1), which is the target point on the HAC (Fig. 4). The HAC concept, which is also used by the Shuttle Orbiter, is an imaginary cylinder that is tangent to the extension of the runway centerline. The point where the HAC and the extension of the runway centerline intersect is called the nominal entry point (NEP). For the glide-back booster guidance algorithm, the HAC is defined with a radius of 21,000 ft and a distance to the runway threshold of 36,800 ft.

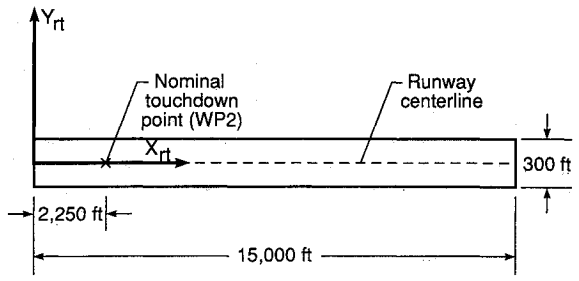

Fig. 5 Runway coordinate system.

Phase 4—Heading Alignment Cylinder

Phase 4 guidance begins when the booster reaches WP1. The booster's roll angle is modulated by feedback to maintain a constant radius turn equal to the radius of the HAC. Throughout phase 4, the angle of attack is maintained at the final phase-3 angle of attack. When the booster has traveled around the cylinder to the point where it is aligned with the runway centerline (NEP), phase 5 is initiated and the booster unrolls.

Phase 5—Approach

Phase 5 begins when the booster is at the NEP and ends when the booster reaches an altitude of 1000 ft. For phase 5, a reference aim point was defined to be 40 ft down the runway, which is approximately 2200 ft short of the desired touchdown position. The booster angle of attack during phase 5 was modulated by feedback to keep the booster flying toward the reference aim point. The roll angle was modulated to maintain the alignment of the booster with the runway centerline.

Phase 6—Flare and Touchdown

At an altitude of 1000 ft, the booster enters phase 6, which is the flare maneuver and touchdown on the runway. As with the Shuttle, the desired touchdown point is approximately 15% of the length down the runway (Fig. 5). A technique was developed that insured that the booster would touch down near the target point, way-point 2 (WP2), while encountering extreme off-nominal conditions. A nominal flare maneuver was found in which the booster had a descent rate of 1.4 ft/s at touchdown on the nominal target point. From this nominal maneuver, a relationship between a reference flight-path angle and altitude profile and the booster's actual flight-path angle and altitude was developed that was used to calculate the booster angle of attack. The roll angle was modulated to maintain the alignment of the booster with the runway centerline.

Nominal Glide-Back Trajectory

For the development of the nominal glide-back trajectory, the 1976 standard atmosphere[11] was used. Figures 6–9 show the nominal glide-back trajectory from the completion of the staging maneuver to touchdown on the runway using the guidance algorithm described in the previous section. The booster requires 523 s to complete the nominal glide-back trajectory. The phase-1 turn is completed during the first 70 s. The booster remains in phase 2 for 50 s while its excess performance is being dissipated. At 120 s into the glide back, the booster initiates the HAC acquisition phase and reaches the HAC at 395 s. At 415 s, the booster comes off the HAC and is aligned with the runway. The flare maneuver starts at 510 s with touchdown occurring at 523 s. The nominal touchdown position is on the centerline, at 2250 ft down the 15,000-ft runway, with a descent rate of 1.4 ft/s. Figure 5 shows the nominal touchdown position in the runway coordinate system.

Figure 6 shows the Mach number and altitude profiles for the nominal glide-back trajectory. The rapid deceleration of

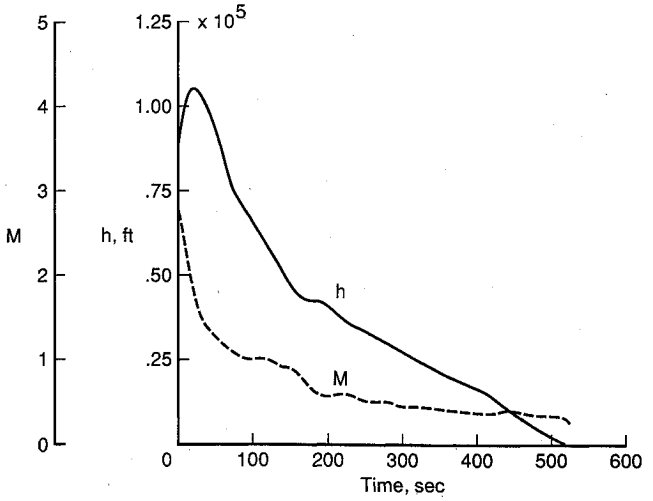

Fig. 6 Nominal Mach number and altitude profiles.

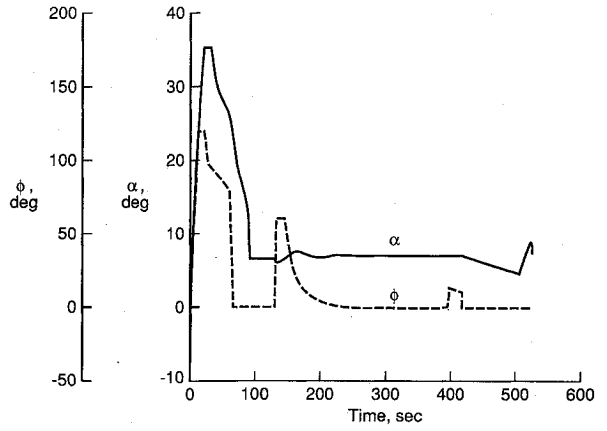

Fig. 7 Nominal roll angle and angle-of-attack profiles.

the booster is seen in the Mach number profile. During the first 100 s, the booster decelerates from Mach 2.8 to below Mach 1.0. The booster remains at subsonic speeds for the remainder of the glide back. The booster reaches a maximum altitude of 110,000 ft at 20 s into the glide back. At 200 s into the glide back, the booster enters into an equilibrium glide until the HAC is reached at 395 s.

The roll angle and angle-of-attack profiles are shown in Fig. 7. The angle of attack reaches a maximum of 35 deg, and the roll angle reaches a maximum of 120 deg during the phase-1 turn. The roll-angle profile shows when the phase-1 turn is completed (70 s), when the booster turns toward the HAC (120 s), and when the booster is on the HAC (395–415 s). The angle-of-attack profile shows that throughout phases 2–4 the booster flies near the desired angle of attack of 6.5 deg.

Figure 8 shows the flight-path angle and normal acceleration profiles. The maximum normal acceleration during the nominal glide back is 2.3 g, which is below the 2.5-g limit. The flight-path angle profile shows that, during the glide back, the flight-path angle varies from a maximum of 30 deg, at staging completion, to a minimum of -45 deg, just after the maximum altitude is attained.

The elevon deflection angle and range profiles are shown in Fig. 9. The elevon deflection angle remains within the limits of $+20$ and -30 deg throughout the glide back. Also, the booster reaches a maximum range of 28 n.mi. from the runway.

Off-Nominal Glide-Back Trajectories

Atmospheric Dispersions

The initial off-nominal conditions used in the guidance sensitivity analysis were constant bias factors applied to the 1976

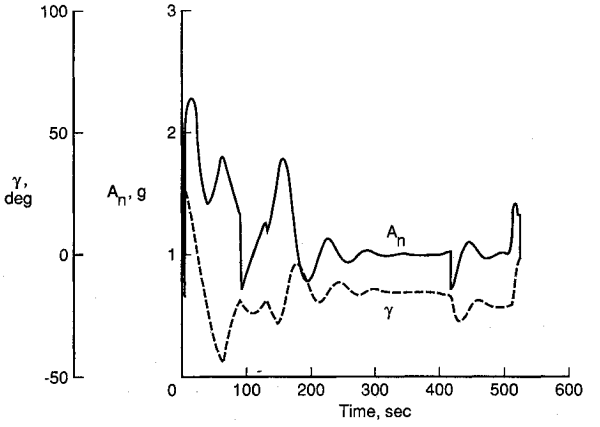

Fig. 8 Nominal flight-path angle and normal acceleration profiles.

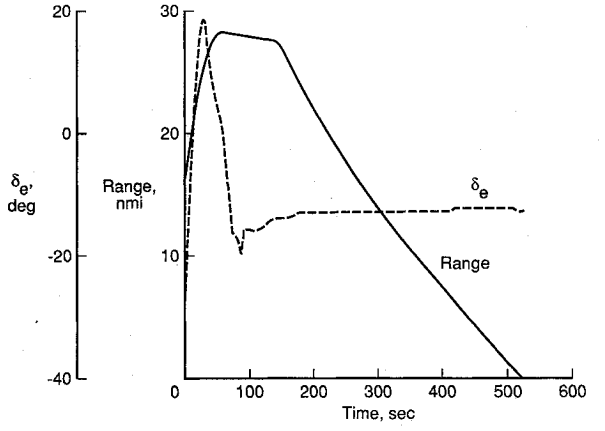

Fig. 9 Nominal elevon deflection angle and range profiles.

standard atmospheric density. The 1976 standard atmospheric density was multiplied by factors of 0.9 and 1.1. Table 3 shows a comparison of these results along with the nominal results. (Refer to Fig. 5 for runway coordinate system definition.) In both cases, the booster landed within 6 ft of the nominal target point and had a lower touchdown velocity (284 ft/s) for the high-density atmosphere, and had a higher touchdown velocity (326 ft/s) for the low-density atmosphere.

Glide-back trajectories were modeled with constant head wind, tail wind, and crosswinds. The wind speed was assumed to be 22 kt. Table 4 shows the results for these four glide-back cases. The constant head and tail winds had a significant effect on the X component of the touchdown velocity, and the constant crosswinds had a significant effect on the Y component of the touchdown velocity. However, each of these four cases landed successfully on the runway. The side velocity at touch-

Table 3 Booster glide-back simulation results for nominal and constant variations in 1976 standard atmospheric density

	X_{rt}, ft	$\dot{X}_{rt}$, ft/s	Y_{rt}, ft	$\dot{Y}_{rt}$, ft/s	$\dot{h}$, ft/s
Nominal	2250	305	0.0	0.0	−1.4
$1.1 \times \rho_{76}$	2256	284	0.0	0.0	−1.3
$0.9 \times \rho_{76}$	2247	326	0.0	0.0	−1.3

Table 4 Booster glide-back simulation results for constant head, tail, and cross winds

	X_{rt}, ft	$\dot{X}_{rt}$, ft/s	Y_{rt}, ft	$\dot{Y}_{rt}$, ft/s	$\dot{h}$, ft/s
Nominal	2250	305	0.0	0.0	−1.4
Head	2140	226	0.0	0.0	−1.4
Tail	2091	379	0.0	0.0	−1.4
Left cross	2239	299	11.7	3.2	−1.4
Right cross	2256	303	−11.4	−3.4	−1.5

down for the two crosswind cases (+3.2 and −3.4 ft/s) results in a sideslip angle of approximately ±1.0 deg, which is well below the ±3-deg sideslip angle the landing gear is designed to handle.

To simulate more realistic atmospheric conditions, mean density profiles and wind profiles for each month of the year were determined using the GRAM program. In addition, 10 perturbed atmospheres and $\pm 3\sigma$ perturbed atmospheres were determined for a single month of the year. July was randomly chosen for these perturbed atmospheres. Figures 10 and 11 show a composite of all of the atmospheres that were generated with the GRAM for use in this study. In Fig. 10, the GRAM atmospheric densities are divided by the 1976 standard atmospheric density to simplify the comparisons. Over the altitude range that the booster covers during the glide back, the GRAM densities range between 6% lower to over 15% higher than the 1976 standard atmospheric density. The east-west component of the winds (Fig. 11) for the GRAM atmospheres varies from 100 ft/s east to 125 ft/s west. The maximum north-south component of the winds is much smaller at < 20 ft/s.

Table 5 shows the results of the glide-back trajectories incorporating each of the monthly mean densities with winds. The landing conditions for all of these trajectories are quite close to the nominal landing conditions. Also, none of the vehicle constraints are violated throughout any of these trajectories. The glide-back trajectories for the 10 perturbed July atmospheres and the $\pm 3\sigma$ variations of the July atmosphere have a similar range in touchdown conditions as the monthly mean densities with winds shown in Table 5.

Aerodynamic Dispersions

Errors in predicted aerodynamics were simulated by multiplying the lift and drag coefficients of the booster by factors of 0.9 and 1.1. The results of these trajectories are shown in Table 6. In the high-drag case and low-lift case, the booster landed closer to the beginning of the runway than any of the other off-nominal cases. The descent rate at touchdown for these two cases is higher than the other off-nominal cases, but still well within the descent rate limit. None of the aerodynamic dispersion cases violated the vehicle constraints. The landing conditions are again very close to the nominal conditions.

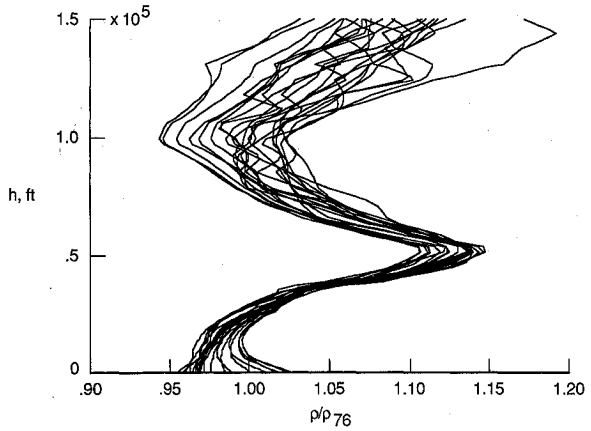

Fig. 10 Monthly and perturbed atmospheric density variations.

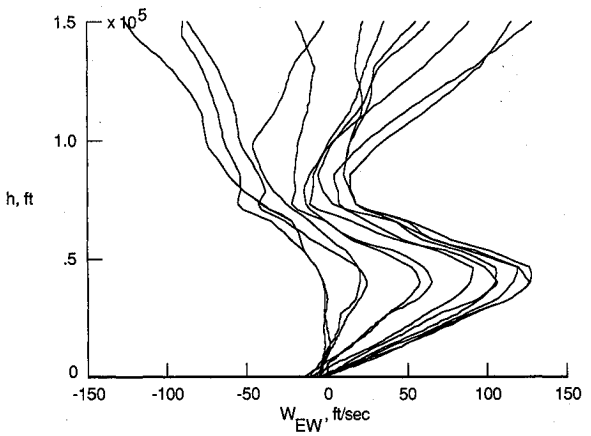

Fig. 11 Monthly east-west wind component variations.

Staging State Dispersions

The errors in the staging conditions were simulated by adding and subtracting 10% to the nominal staging altitude, velocity, and flight-path angle. Table 7 summarizes the results for these glide-back trajectories. The guidance algorithm was able to adjust to these errors in staging conditions and land the booster close to the nominal position and velocity and remain within the vehicle constraints, except for the case in which the staging altitude is 10% low. For this case, the normal accelera-

Table 5 Booster glide-back simulation results for GRAM atmospheric density variations

	X_{rt}, ft	$\dot{X}_{rt}$, ft/s	Y_{rt}, ft	$\dot{Y}_{rt}$, ft/s	$\dot{h}$, ft/s
Nominal	2250	305	0.0	0.0	−1.4
January	2134	273	−1.8	−0.5	−1.4
February	2123	268	−1.2	−0.3	−1.4
March	2108	273	−0.3	−0.1	−1.3
April	2156	288	0.4	0.1	−1.2
May	2250	308	−0.4	−0.1	−1.4
June	2241	323	−0.6	−0.3	−1.4
July	2235	326	0.2	0.0	−1.5
August	2242	324	−0.4	−0.2	−1.4
September	2254	321	−2.4	−0.8	−1.3
October	2234	309	−3.8	−1.1	−1.4
November	2197	291	−3.8	−1.0	−1.2
December	2149	278	−2.6	−0.7	−1.3

Table 6 Booster glide-back simulation results for constant variations in predicted aerodynamics

	X_{rt}, ft	$\dot{X}_{rt}$, ft/s	Y_{rt}, ft	$\dot{Y}_{rt}$, ft/s	$\dot{h}$, ft/s
Nominal	2250	305	0.0	0.0	−1.4
Drag					
$1.1 \times C_{D,nom}$	2036	259	0.0	0.0	−1.7
$0.9 \times C_{D,nom}$	2186	364	0.0	0.0	−1.0
Lift					
$1.1 \times C_{L,nom}$	2219	335	0.0	0.0	−1.4
$0.9 \times C_{L,nom}$	1931	263	0.0	0.0	−1.7

Table 7 Booster glide-back simulation results for variations in predicted staging parameters

	X_{rt}, ft	$\dot{X}_{rt}$, ft/s	Y_{rt}, ft	$\dot{Y}_{rt}$, ft/s	$\dot{h}$, ft/s
Nominal	2250	305	0.0	0.0	−1.4
Staging altitude					
10% high	2239	303	0.0	0.0	−1.4
10% low	2247	303	0.0	0.0	−1.4
Staging velocity					
10% high	2245	302	0.0	0.0	−1.4
10% low	2246	306	0.0	0.0	−1.4
Staging flight path angle					
10% high	2233	305	0.0	0.0	−1.4
10% low	2252	306	0.0	0.0	−1.4

Table 8 Range of touchdown conditions for glide-back simulations

	Minimum	Nominal	Maximum
Total glide-back time, s	483	525	651
X_{rt}, ft	1931	2250	2272
$\dot{X}_{rt}$, ft/s	226	305	379
Y_{rt}, ft	−11.4	0	11.6
$\dot{Y}_{rt}$, ft/s	−3.4	0	3.2
$\dot{h}$, ft/s	−1.0	−1.4	−1.7

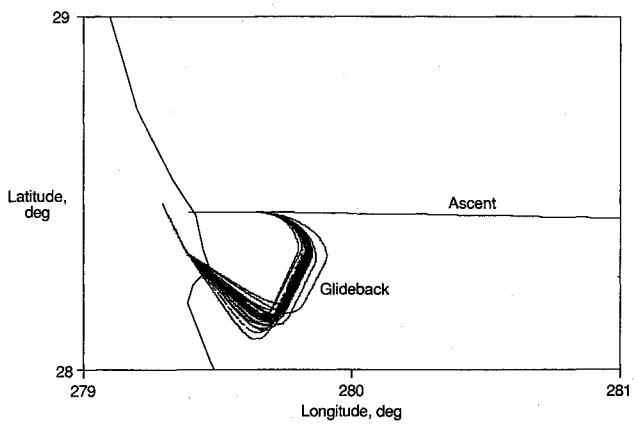

Fig. 12 Off-nominal latitude vs longitudinal profiles.

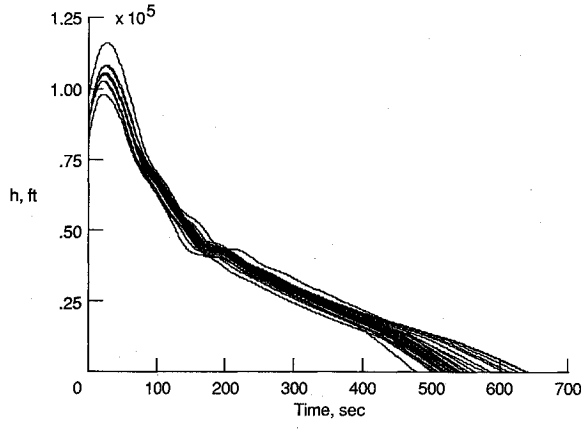

Fig. 13 Off-nominal altitude profiles.

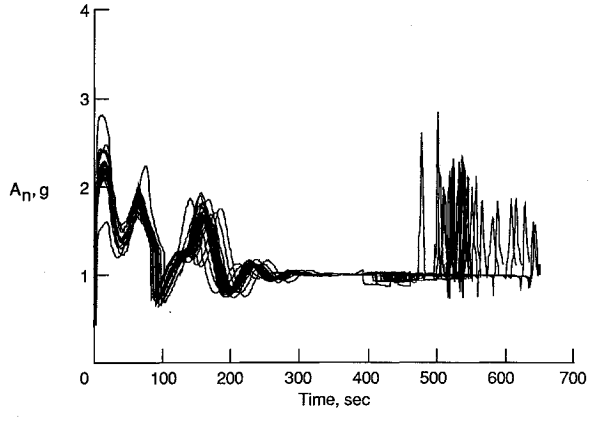

Fig. 14 Off-nominal normal acceleration profiles.

tion reached a maximum of 2.75 *g* during the phase-1 turning maneuver. It was determined that, if the low altitude error is limited to 6%, the normal acceleration limit is not violated.

Summary of Off-Nominal Glide-Back Trajectories

Table 8 shows the range in touchdown conditions for all of the off-nominal cases. The time at touchdown varied widely from 483 to 651 s. The booster's touchdown position varied from 1931 to 2272 ft down the runway and was within 12 ft of the runway's centerline. The velocity at touchdown varied from 226 to 379 ft/s with the side velocity < 3.4 ft/s. All of the off-nominal cases had a descent rate at touchdown below 1.7 ft/s.

All of the trajectories discussed in this section are plotted together in Figs. 12–16. Figure 12 shows the wide range of paths the booster followed to reach the HAC, and Fig. 13

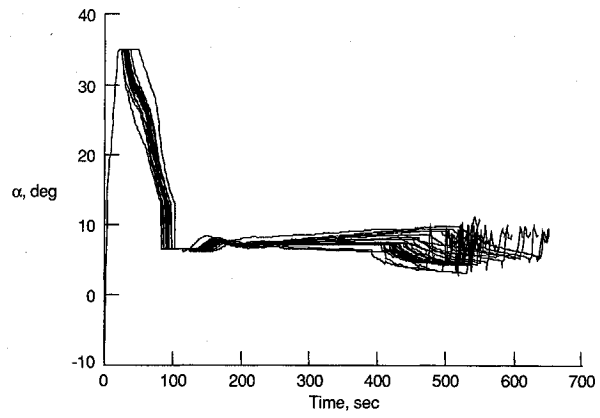

Fig. 15 Off-nominal angle-of-attack profiles.

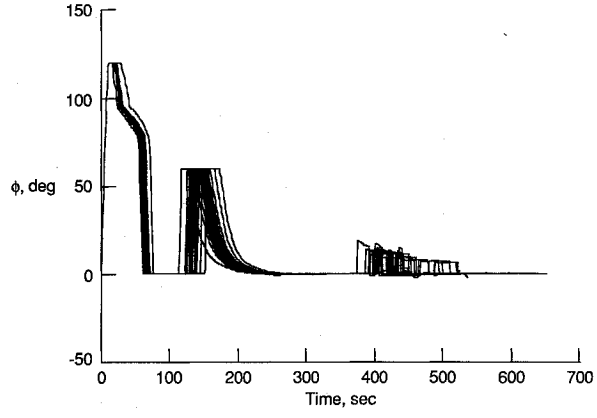

Fig. 16 Off-nominal roll angle profiles.

shows the corresponding altitude profiles. The normal acceleration profiles (Fig. 14) show that all but one off-nominal case remained below the 2.5-*g* normal acceleration constraint. This particular case, the 10% low initial altitude case, was discussed in the previous section. The angle-of-attack histories (Fig. 15) varied significantly depending on the off-nominal conditions but never reached the upper and lower limits of +10 and +5 deg during phases 2–5. The individual roll angle histories (Fig. 16) are similar but show that the phases occur at widely varying times. The elevon deflections remained within the limits of +20 and −30 deg during all of the off-nominal glide-back trajectories.

Conclusions

Many concepts that could replace the current Shuttle launch system are currently being studied. One promising concept is a two-stage, fully reusable, vertical-takeoff launch vehicle that utilizes a glide-back booster. One of the major design issues for this class of vehicle that has not been addressed previously has been analyzed in this paper. A guidance scheme for the booster's glide back to the launch site was developed. The guidance algorithm was incorporated into a three-degree-of-freedom trajectory program with longitudinal static trim so that the elevon deflections required for trim could be calculated. Glide-back simulations were modeled with a variety of off-nominal atmospheric, aerodynamic, and staging conditions with the booster remaining within 320 ft of the nominal touchdown point and a descent rate of < 1.7 ft/s. This analysis has shown that the booster unpowered glide back is a viable maneuver for a two-stage system that stages at Mach 3.

References

[1]Freeman, D. C., "The New Space Transportation Begins Today," *Astronautics and Aeronautics*, Vol. 21, No. 6, 1983, pp. 36–37, 48.

[2]Martin, J. A., "Orbit on Demand: In This Century If Pushed,"

Aerospace America, Vol. 23, No. 2, 1985, pp. 46–48.

[3]Talay, T. A., "Shuttle II Progress Report," *Proceedings of the Twenty-Fourth Space Congress,* April 21–24, 1987, Canaveral Council of Technical Societies, Cocoa Beach, FL.

[4]Talay, T. A., and Morris, W. D., "Advanced Manned Launch Systems," European Aerospace Conference, Paper 89-17, May 1989.

[5]Naftel, J. C., and Powell, R. W., "Flight Analysis for a Two-Stage Launch Vehicle with a Glideback Booster," *Journal of Guidance, Control, and Dynamics,* Vol. 8, No. 3, 1985, pp. 340–343.

[6]Powell, R. W., Naftel, J. C., and Cruz, C. I., "Flight Control Issues of the Next Generation Space Transportation Launch Vehicles," *AGARD Conference Proceedings No. 489,* Nov. 1989.

[7]Freeman, D. C., and Fournier, R. H., "Static Aerodynamic Characteristics of a Winged Single-Stage-to-Orbit Vehicle at Mach Numbers from 0.3 to 4.63," NASA TP-1233, Aug. 1978.

[8]Brauer, G. L., Cornick, D. E., and Stevenson, R., "Capabilities and Applications of the Program to Optimize Simulated Trajectories (POST)," NASA CR-2770, Feb. 1977.

[9]Justus, C. G., Fletcher, G. R., Gramling, F. E., and Pace, W. B., "The NASA/MSFC Global Reference Atmospheric Model—Mod 3 (With Spherical Harmonic Wind Model)," NASA CR-3256, 1980.

[10]Justus, C. G., Alyea, F. N., Cunnold, D. M., and Johnson, D. L., "Gram-88, Improvements in the Perturbation Simulations of the Global Reference Atmospheric Model," ES44-11-9-88, NASA Grant NAG8-078, Georgia Tech. Project G-35-685, Nov. 1988.

[11]*U.S. Standard Atmosphere, 1976,* NOAA S/T 76-1562, Oct. 1976.

James A. Martin
Associate Editor